JOURNAL OF CATALYSIS 118, 147–163 (1989)

Non-Faradaic Electrochemical Modification of Catalytic Activity

2. The Case of Methanol Dehydrogenation and Decomposition on Ag

S. NEOPHYTIDES AND C. G. VAYENAS[1]

Institute of Chemical Engineering and High Temperature Chemical Processes, Department of Chemical Engineering, University of Patras, Patras, Greece

Received July 13, 1988; revised October 17, 1988

It was found that the catalytic activity and selectivity of polycrystalline Ag for the dehydrogenation and decomposition of CH_3OH can be markedly affected by electrochemically pumping oxygen anions from the catalyst surface via stabilized zirconia solid electrolyte cells. The steady-state increases in catalytic rates are typically a factor of 20 higher than the rate of O^{2-} transfer from the catalyst surface. Oxygen anion pumping causes up to sixfold increases in the rates of production of H_2CO, CO, and CH_4 and induces significant changes in product selectivity. Over a wide range of conditions the rates of the catalytic reactions increase exponentially with catalyst–solid electrolyte interface overpotential η, which is proportional to the induced change in catalyst work function. The phenomena are reversible and show that catalyst work function and catalytic activity and selectivity can be varied deliberately by adjusting the catalyst potential. The observed non-Faradaic rate enhancement for this catalytic system can be interpreted by taking into account the decrease in catalyst work function with decreasing catalyst potential and the consequent changes in the strength of chemisorptive bonds.

INTRODUCTION

Solid electrolyte cells can be used in several ways to study and to influence catalytic phenomena on metals. Progress in this area has been reviewed recently (*1, 2*). The first studies focused mostly on passive potentiometric measurements of the activity of oxygen on porous metal catalyst films. This technique of solid electrolyte potentiometry (SEP) has been used in conjunction with kinetic measurements to study a number of catalytic reactions on metals (*3–6*). It is particularly suitable for the study of oscillatory reactions (*4, 7–10*).

In recent years it has been found that the catalytic activity and selectivity of metal catalysts can be altered dramatically and in a reversible manner by electrochemically pumping oxygen anions (O^{2-}) to or from catalyst surfaces. In this "active" mode of operation a current I is applied to cells of the type

gaseous reactants, metal catalyst $|ZrO_2(8\ mol\%\ Y_2O_3)|M,O_2$ (1)

and O^{2-} are pumped to or from the catalyst surface at a rate $I/2F$, where F is Faraday's constant. The metal (M) catalyzes the reaction

$$O_2(g) + 4e^- \leftrightarrows 2O^{2-} \qquad (2)$$

and serves as a means of supplying or removing O^{2-} to or from the porous metal catalyst film through the gas-impervious stabilized zirconia solid electrolyte.

Oxygen anion removal from the catalyst surface has been found to significantly enhance the rate of NO decomposition on Pt and Au (*11, 12*) and the rate of CO hydrogenation on transition metals (*13, 14*). In the latter case the rate increase has been attributed to an enhancement in the rate of dissociation of chemisorbed CO.

It is useful to define an enhancement factor Λ from

$$\Lambda = \Delta r/(I/2F) \qquad (3)$$

[1] To whom correspondence should be addressed.

0021-9517/89 $3.00

where Δr is the change in *catalytic* reaction rate and $I/2F$ is the rate of O^{2-} transport to or from the catalyst surface. Throughout this paper and as in previous ones (*1, 15, 20*) we have defined the current I to be positive when O^{2-} is pumped *to* the catalyst and negative when O^{2-} is pumped *from* the catalyst. The published results for the cases of NO decomposition on Pt and Au (*11, 12*) show that $|\Lambda| \approx 1$, i.e., the observed behavior was purely Faradaic.

In several recent studies, $|\Lambda|$ values well in excess of unity have been reported for a variety of catalytic reactions. These include the partial oxidation of ethylene and propylene on Ag (*16–18*), where significant changes in product selectivity were also observed, the oxidation of CO on Pt (*19*), and the complete oxidation of ethylene on Pt, where Λ values as high as 3×10^5 were measured with a concomitant 50-fold increase in catalytic reaction rate (*15, 20*). The term non-Faradaic electrochemical modification of catalytic activity (NEMCA) was proposed to describe this new phenomenon (*15, 20*). It should be emphasized that the term non-Faradaic simply implies that the change in the rate of the *catalytic* reaction exceeds the rate of O^{2-} transport which, of course, always equals the rate of the *electrocatalytic* reaction (2).

One of the central findings of the recent investigations of the NEMCA effect (*15, 20*) is that the most significant parameters in describing and understanding the effect are the catalyst–solid electrolyte activation overpotential η and the catalyst potential, relative to the reference electrode, V_{WR}. It was found that over wide ranges of V_{WR} the catalytic reaction rate r changes exponentially with V_{WR} according to

$$\ln(r/r_o) = \alpha F(V_{WR} - V^*_{WR})/RT \qquad (4)$$

where r_o is the regular (open-circuit) catalytic rate and α and V^*_{WR} are constants. This behavior was explained by considering the change in the heats of adsorption of chemisorbed species caused by changes in the catalyst work function as the catalyst potential changes (*15, 20*).

In the present communication the NEMCA effect is examined for the reactions of methanol dehydrogenation and decomposition on Ag. Similarly to previous studies (*15, 20*) it is found that over a range of catalyst potential the rates of the dehydrogenation, decomposition, and methane formation reactions depend exponentially on catalyst potential. However, an important difference with previous reactions studied is that the rates increase exponentially with decreasing catalyst potential, i.e., when oxygen anions are pumped *from* the catalyst surface. This behavior can be understood by considering that oxygen anion removal from the catalyst leads to a decrease in catalyst work function and to a concomitant increase in chemisorptive bond strengths which results in an enhancement in the rates of dehydrogenation and decomposition.

EXPERIMENTAL

The experimental apparatus is shown schematically in Fig. 1. An ultrapure (99.999%) He stream was saturated with CH_3OH by being sparged through a thermostated saturator containing liquid CH_3OH. The reactor inlet CH_3OH concentration was controlled by mixing the saturated He stream with a second ultrapure He stream. A TC detector (Gow-Mac 50-152) was used to continuously monitor the reactor inlet CH_3OH concentration. Reactants and products were analyzed by on-line gas chromatography using a Perkin–Elmer Sigma 300 gas chromatograph with a TC detector and a Perkin–Elmer LCI-100 integrator. A Chromosorb 107 glass column was used to separate CH_3OH, H_2CO, and CO_2 and a molecular sieve 5A column to separate O_2,CO, and CH_4. Relative response factors based on N_2 were measured for each component separately and are given in Table 1. The inlet CH_3OH partial pressure was typically on the order of 5×10^{-2} bar. The feed also contained small

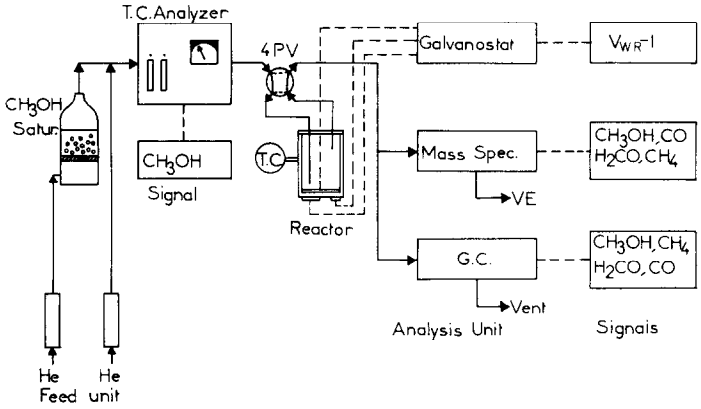

FIG. 1. Schematic diagram of the apparatus.

amounts of O_2 and H_2O, typically 9×10^{-5} and 3.5×10^{-4} bar, respectively.

A Balzers QMG 311 mass spectrometer with a continuous gas-sampling system and a QDP data processor were also used for reactant and product analysis. This permitted continuous monitoring of the exit concentrations of CH_3OH, H_2CO, CO, CH_4, H_2, and H_2O. All gas lines and valves were heated at 100°C using heating tapes to prevent condensation of CH_3OH, H_2CO, and H_2O and polymerization of H_2CO. The carbon mass balance was typically found to close within 0.5%. The oxygen mass balance was also found to close within 1%. Due to the strong hydrogen background signal in the vacuum system resulting from the turbomolecular pumping unit, no systematic study was made of the hydrogen mass balance closure, which, however, is almost guaranteed by the very good closure of the carbon and oxygen mass balances.

The atmospheric pressure yttria-stabilized zirconia continuous-flow reactor shown schematically in Fig. 2 has a volume of 30 cm^3 and has been described in detail in previous communications (*7, 9, 15, 19*). Within the flow rate range used in this investigation, i.e., typically 90 to 110 cm^3 STP/min, the reactor has been shown to behave like a CSTR by measurement of its residence time distribution with an IR CO_2 analyzer (*7*).

Porous Ag catalyst films were deposited on the inside bottom of the stabilized zirconia tube as described previously (*3–5, 16–18*), i.e., by using thin coatings of a Ag solution in butyl acetate followed by drying and calcining at 650°C. Porous Ag films deposited in this mode have thickness on the or-

TABLE 1

Relative Response Factors

O_2	1.00
CO	1.00
CH_3OH	0.88
H_2CO	1.175
CH_4	1.09
H_2O	1.70

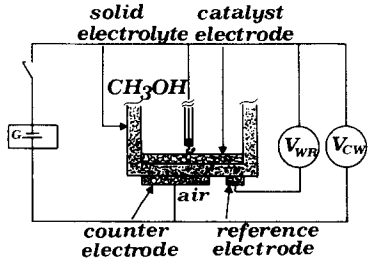

FIG. 2. Catalyst and auxiliary electrode configuration. G, galvanostat–potentiostat.

TABLE 2

Catalyst	Reactive oxygen uptake of catalyst electrode (N_o/g-at. O)	Exchange current density at P_M = 5×10^{-2} bar [I_o (μA/cm^2)]	Relaxation time (s)	
			Experimental (τ)	Computed ($2FN_o/I$)
1	5.5×10^{-6}	67 (650°C)	—	—
2	6.9×10^{-6}	45 (663°C)	350–700 ($I = -2$ mA)	664

der of 5 μm and have been found by *ex situ* AES to be fairly clean (*3*). Their superficial surface area is 2 cm^2 and their true surface area as measured by a surface titration technique described previously using O_2 and CO (*7, 9, 16*) is on the order of 2000 cm^2. Three porous Ag films were used in the course of the experiments and all showed qualitatively the same kinetic behavior. However, detailed kinetic and electrokinetic investigation was done with two of them. Their reactive oxygen uptake at 450°C, estimated surface area, and exchange current density characteristics are given in Table 2.

Electrochemical measurements. The three-electrode system shown in Fig. 2 and described in previous communications (*15, 19, 21*) was used to measure the catalyst–solid electrolyte activation overpotential η and the exchange current I_o.

The two porous Ag films deposited on the outside bottom wall of the stabilized zirconia tube were exposed to ambient air. One had a superficial surface area of 1.2 cm^2 and served as the counterelectrode; the other with a superficial area of 0.1 cm^2 served as a reference electrode.

Under open-circuit conditions the porous Ag film exposed to the reactants (working electrode) functions as a regular catalyst. When the circuit is closed and a galvanostat (in this work an AMEL 553 galvanostat–potentiostat) is used to impose a constant current I between the working and counterelectrodes, oxygen anions O^{2-} are transferred to or from the catalyst at a rate $I/2F$, where F is a Faraday's constant. At the same time the catalyst potential relative to the reference electrode V'_{WR} deviates from its open-circuit emf value $V^o_{WR} = V_{WR(I=0)}$, which is on the order of $-1V$ for this system. The difference $V'_{WR} - V^o_{WR}$ equals theoretically the overpotential η at the catalyst–solid electrolyte interface (*15, 19, 21, 22*). In practice the reference electrode is never ideal and V'_{WR} always contains a nonzero ohmic component. This component, which was typically of order 10–30 mV in our system, was measured using the current interruption technique in conjunction with a Hameg HM 205 memory oscilloscope and was subtracted from V'_{WR} to obtain the IR-free catalyst potential V_{WR}. One can then compute η from

$$\eta = V_{WR} - V^o_{WR}. \tag{5}$$

By measuring η as a function of the current I, or equivalently current density $i = I/A$, where A is the solid electrolyte surface area ($\approx$1.5–2.0 cm^2 in our system) and by using the classical Butler–Volmer equation

$$I/I_o = \exp(\alpha_a F\eta/RT) - \exp(-\alpha c F\eta/RT) \tag{6}$$

one can determine the values of the exchange current I_o and of the anodic and cathodic transfer coefficients α_a and α_c. This is usually done by using the high-field approximation ($|\eta| > 100$ mV), in which case Eq. (6) reduces to

$$\ln(I/I_o) = \alpha_a F\eta/RT \tag{7}$$

for anodic ($I > 0$, $\eta > 0$) currents and

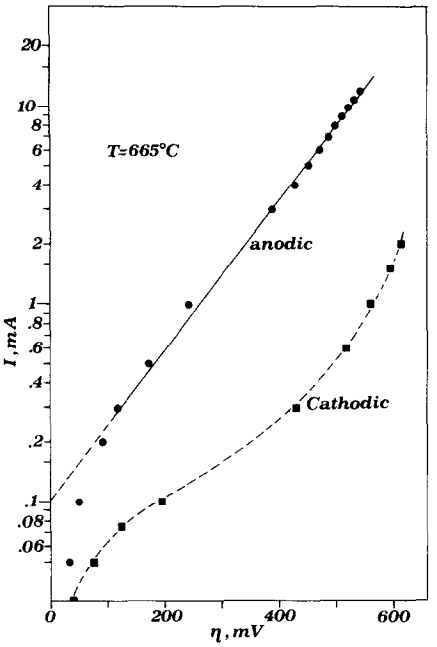

FIG. 3. Tafel plots of the catalyst–solid electrolyte interface. $P_M = 5 \times 10^{-2}$ bar.

$$\ln(-I/I_o) = -\alpha_c F\eta/RT \qquad (8)$$

for cathodic operation. Thus, by plotting ln-I versus η (Tafel plot) one obtains I_o, α_a, and α_c. Such Tafel plots are shown in Fig. 3.

The exchange current density $i_o = I_o/A$ is a measure of the electrocatalytic activity of the catalyst–solid electrode interface for the reaction

$$O^{2-} \leftrightarrows O^{\delta-}(a) + (2 - \delta_-)e \qquad (9)$$

where $O^{\delta-}(a)$ is oxygen chemisorbed on the Ag catalyst in the vicinity of the three phase boundaries between the catalyst, the solid electrolyte, and the gas phase. The parameter i_o expresses the rates of the forward and backward reactions (9) which are equal when $I = 0$. High i_o values, e.g., 10^{-3} A/cm^2, indicate a nonpolarizable metal–solid electrolyte interface, while low i_o values, e.g., 10^{-9} A/cm^2, are indicative of a highly polarizable interface.

The parameters i_o, α_a, and α_c refer to the *electrocatalytic* reaction (9) the rate of which, as already mentioned, can be 15–20 times smaller than the induced changes in the *catalytic* rate of CH_3OH consumption, which takes place over the entire Ag catalyst surface. However, these parameters are important in understanding the electrocatalytically induced change in catalytic activity. It is the overpotential η that connects the *electrocatalytic* reaction rate, which equals the rate of O^{2-} transport through the electrolyte to or from the catalyst, with the induced change in the *catalytic* activity of Ag, which, as recently shown (*15, 20*) and as discussed below, is proportional to the induced change in the average work function of the catalyst.

RESULTS

Regular (Open-Circuit) Catalytic Behavior

The kinetics of CH_3OH dehydrogenation to H_2CO (r_{H_2CO}), decomposition to CO and H_2 (r_{CO}), and conversion to CH_4 (r_{CH_4}) were studied at temperatures from 600 to 680°C and CH_3OH partial pressures up to 0.07 bar, first under open-circuit conditions. Although the reactor behaves as a CSTR, the total CH_3OH conversion was deliberately maintained below 20% in all the experiments to maintain differential reactor conditions and limit the occurrence of consecutive reactions, such as H_2CO decomposition and CO hydrogenation to CH_4. Figure 4 shows typical results for the dependence of the rate of formaldehyde production r_{H_2CO} on the partial pressure of methanol P_M. It was found that r_{H_2CO} can be approximated well by simple Langmuir-type rate expressions, i.e.,

$$r_{o,H_2CO} = K_{o,H_2CO}K_{o,M}P_M/(1 + K_{o,M}P_M) \qquad (10)$$

with

$$K_{o,M} = 0.032 \exp(8800/T) \text{ bar}^{-1} \qquad (11)$$

$$K_{o,H_2CO} = 14.7 \exp(-7050/T) \text{ s}^{-1} \qquad (12)$$

where the subscript o is used to denote regular, i.e., open-circuit, catalytic behavior, and the kinetic constant K_{o,H_2CO} has been

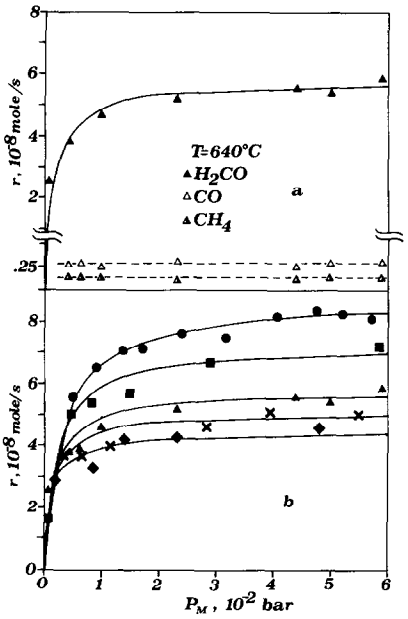

FIG. 4. Effect of methanol partial pressure on the open-circuit kinetics of formation of H_2CO, CO, and CH_4 at 640°C (a) and on the open-circuit kinetics of H_2CO formation at various temperatures (b). ◆, T = 600°C; X, T = 625°C; ▲, T = 640°C; ■, T = 663°C; ●, T = 679°C. Solid lines from equations (10)–(16). Catalyst 2.

expressed in s^{-1} by using the reactive oxygen uptake of the catalyst, i.e., $N_o = 9.4 \times 10^{-6}$ g-at. The solid curves in Fig. 4 were obtained from the kinetic expression (10). The open-circuit rates of CO and CH_4 formation, i.e., $r_{o,CO}$ and r_{o,CH_4}, respectively, are also zero order in methanol for CH_3OH partial pressures above 5×10^{-3} bar and can be approximated reasonably well by

$$r_{o,CO} = K_{o,CO}K_{o,M}P_M/(1 + K_{o,M}P_M) \quad (13)$$

$$r_{o,CH_4} = K_{o,CH_4}K_{o,M}P_M/(1 + K_{o,M}P_M) \quad (14)$$

with

$$K_{o,CO} = 0.41 \exp(-6500/T)\ s^{-1} \quad (15)$$

$$K_{o,CH_4} = 10.2 \exp(-10{,}000/T)\ s^{-1} \quad (16)$$

The selectivities to H_2CO, CO, and CH_4, defined from

$$S_{H_2CO} = r_{H_2CO}/r_{CH_3OH}, \quad S_{CO} = r_{CO}/r_{CH_3OH},$$
$$S_{CH_4} = r_{CH_4}/r_{CH_3OH},$$

where r_{CH_3OH} is the rate of CH_3OH consumption, are typically of order S_{o,H_2CO} = 85–90%, $S_{o,CO}$ = 7–11%, and S_{o,CH_4} = 3–5% over the temperature range investigated and are essentially independent from the partial pressure of methanol, P_M. Although the kinetics and mechanism of CH_3OH oxidation on Ag have been studied extensively, e.g., Refs. (*23–25*), there is, to our knowledge, no previously published detailed investigation of the kinetics of the above reactions in the absence or presence of trace amounts of oxygen.

A limited study of the effect of flow rate or residence time showed that S_{H_2CO}, S_{CO}, and S_{CH_4} are essentially independent from residence time or CH_3OH conversion to the extent that the latter does not exceed 20%. Consequently, over the range of the present investigation, the three reactions

$$CH_3OH \rightarrow H_2CO + H_2 \quad (17)$$

$$CH_3OH \rightarrow CO + 2H_2 \quad (18)$$

$$CH_3OH + H_2 \rightarrow CH_4 + H_2O \quad (19)$$

can be viewed macroscopically and kinetically as three parallel reactions, the rates of which depend essentially only on P_M and temperature.

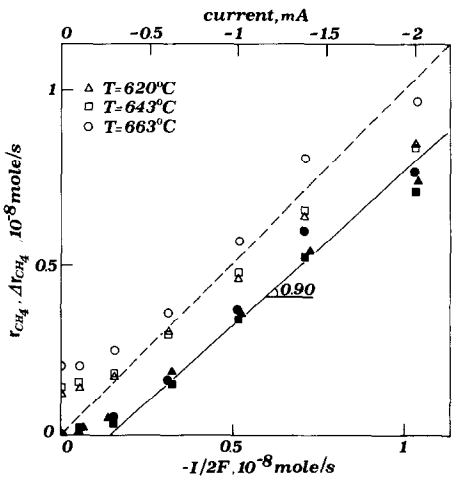

FIG. 5. Effect of current on the rate (open symbols) and on the increase in the rate (filled symbols) of methane formation. The dashed line corresponds to the stoichiometry of reaction (21).

Electrocatalytic Behavior

Figure 3 shows typical current–overpotential (Tafel) plots. One curve corresponds to anodic operation and exhibits clear Tafel behavior with an anodic transfer coefficient $\alpha_a = 0.75 \pm 0.05$. A linear Tafel plot implies that the coverages of kinetically important adsorbed species remain practically constant. It should be noted that anodic operation, i.e., oxygen anions being pumped *to* the catalyst, was found to cause only Faradaic changes in the rates of the catalytic reactions. The temperature dependence of the exchange current density i_o extracted from the anodic Tafel plots corresponds to an activation energy of 45 kcal/mol.

The second curve corresponds to cathodic operation, i.e., O^{2-} removal *from* the catalyst, and exhibits no clear Tafel, i.e., linear, region. This behavior can be understood as follows.

At low (<100 μA) currents, the cathodic electrocatalytic reaction is

$$O^{\delta-}(a) + (2 - \delta_-)e \rightarrow O^{2-} \qquad (20)$$

However, O_2 is present only in trace amounts in the reactor, since its inlet partial pressure is on the order of 9×10^{-5} bar and since most of it reacts with H_2 produced by the catalytic reactions (17) and (18). Consequently, a plateau (limiting current) is approached in the ln I versus $|\eta|$ plot. At higher (>100 μA) cathodic currents a second electrocatalytic reaction starts taking place in parallel with reaction (20), i.e.,

$$CH_3OH + 2e \rightarrow CH_4 + O^{2-} \qquad (21)$$

and this leads to the observed near-exponential increase in current with $|\eta|$ shown in Fig. 3 for high cathodic currents. The fact that oxygen abstraction from CH_3OH is indeed taking place by the electrocatalytic reaction (21) at high current densities is shown conclusively in Fig. 5, where the increase in the rate of CH_4 formation Δr_{CH_4} is plotted versus the rate of O^{2-} removal from the catalyst, $I/2F$, for the same conditions as in Fig. 3 and for two additional temperatures. As shown on the figure the slope of Δr_{CH_4} versus $I/2F$ is near unity at high current densities. The difference between $I/2F$ and Δr_{CH_4} corresponds, for all currents, to the rate of O^{2-} formation from reaction (20).

The NEMCA Effect: Transients

Figure 6 shows a typical galvanostatic transient, i.e., a typical catalytic rate tran-

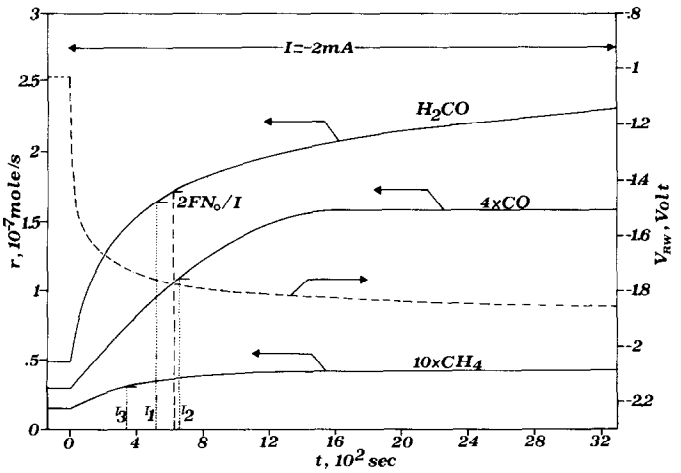

FIG. 6. Rate and catalyst potential response to a step change in applied current. Comparison of experimental (τ) and computed ($2FN_o/I$) relaxation time constants. T = 660°C, $P_M = 5.2 \times 10^{-2}$ bar, catalyst 2; see text for discussion.

sient when a constant negative current, I, i.e., a constant flux of O^{2-} equal to $I/2F$, is removed from the catalyst. The same figure shows the corresponding catalyst potential V_{WR} transient.

At the start of the experiment the circuit is open and the rates of H_2CO, CO, and CH_4 production are $r_{o,H_2CO} = 4.9 \times 10^{-8}$ mol/s, $r_{o,CO} = 7.6 \times 10^{-9}$ mol/s, and $r_{o,CH_4} = 1.5 \times 10^{-9}$ mol/s, respectively. At time $t = 0$ the galvanostat is used to apply a current $I = -2$ mA with a corresponding rate of oxygen transfer from the catalyst $G_o = I/(2F) = 1.04 \times 10^{-8}$ g-at./s. This causes a 380% increase in r_{H_2CO} and a 413% increase in r_{CO}. The corresponding enhancement factors are $\Lambda_{H_2CO} = -17.5$, $\Lambda_{CO} = -3$. There is also a 190% increase in r_{CH_4} with a corresponding enhancement factor $\Lambda_{CH_4} = -0.3$, but this rate increase, as previously mentioned, is mostly Faradaic and due to the electrocatalytic reaction (21). The rate relaxation time constants τ, defined as the time required for the rate increase Δr to reach 63% of its final value, are shown in Fig. 6 to vary between 350 and 700 s, in very good agreement with $2FN_o/I = 664$ s, which is the time required to remove a monolayer of $O^{\delta-}$ from the catalyst surface through the O^{2-} conducting solid electrolyte.

It is worth noting in Fig. 6 that the relaxation time constant τ_3 for CH_4 formation is substantially shorter than the time constants τ_1, and τ_2 for H_2CO and CO formation, respectively. This must be due to the fact that CH_4 is formed not only from the catalytic reaction (19) but also from the electrocatalytic reaction (21) which is expected to have a negligible time constant during a galvanostatic transient.

As shown in Fig. 6 the catalyst potential V_{WR} changes from its open-circuit value of $V^o_{WR} = -1030$ mV to a steady-state value of -1860 mV. The observed changes in the rates and in V_{WR} are quite reversible. Upon current interruption r_{H_2CO}, r_{CO}, r_{CH_4}, and V_{WR} all return to their open-circuit values with a time constant four to five times longer than τ.

Positive current application, i.e., O^{2-} pumping to the catalyst, has only a Faradaic ($\Lambda \leq 1$) effect on the rates for this reaction system.

Steady-State Effect of Current

Figure 7 shows the effect of current on the steady-state increase in the rate of H_2CO formation and on S_{H_2CO}. Increasing negative current enhances the rate of H_2CO formation but causes a decrease in S_{H_2CO}. Enhancement factors Λ_{H_2CO} on the order of -15 are typically obtained. As shown in the Discussion and as recently described (*15–20*) the magnitude of Λ is basically determined by the magnitudes of the open-circuit rate and of the exchange current density i_o.

Effect of Overpotential

Figure 8 shows the effect of the catalyst–solid electrolyte overpotential η on the rates of formation of H_2CO, CO, and CH_4. It can be seen that small negative η values have no effect on the rate. However, as η becomes more negative, r_{H_2CO}, r_{CO}, and r_{CH_4} start to increase exponentially with decreasing η. One can approximate this kinetic behavior by

$$\ln(r_{H_2CO}/r_{o,H_2CO}) = A_{H_2CO}(\eta^*_{H_2CO} - \eta) \quad \eta < \eta^*_{H_2CO} \tag{22a}$$

$$\ln(r_{CO}/r_{o,CO}) = A_{CO}(\eta^*_{CO} - \eta) \quad \eta < \eta^*_{CO} \tag{22b}$$

$$\ln(r_{CH_4}/r_{o,CH_4}) = A_{CH_4}(\eta^*_{CH_4} - \eta) \quad \eta < \eta^*_{CH_4} \tag{22c}$$

where A_{H_2CO}, A_{CO}, A_{CH_4}, $\eta^*_{H_2CO}$, η^*_{CO}, and $\eta^*_{CH_4}$ are temperature-dependent parameters. The exponential dependence of the rates of H_2CO and CO formation on overpotential is similar to that reported recently for the oxidation of C_2H_4 on Pt (*15, 20*). The only difference is in the sign of η, i.e., in the present case the rates increase with decreasing η. As shown in the Discussion it is $\eta = \Delta\Phi$; consequently the catalytic rates increase with decreasing catalyst work function.

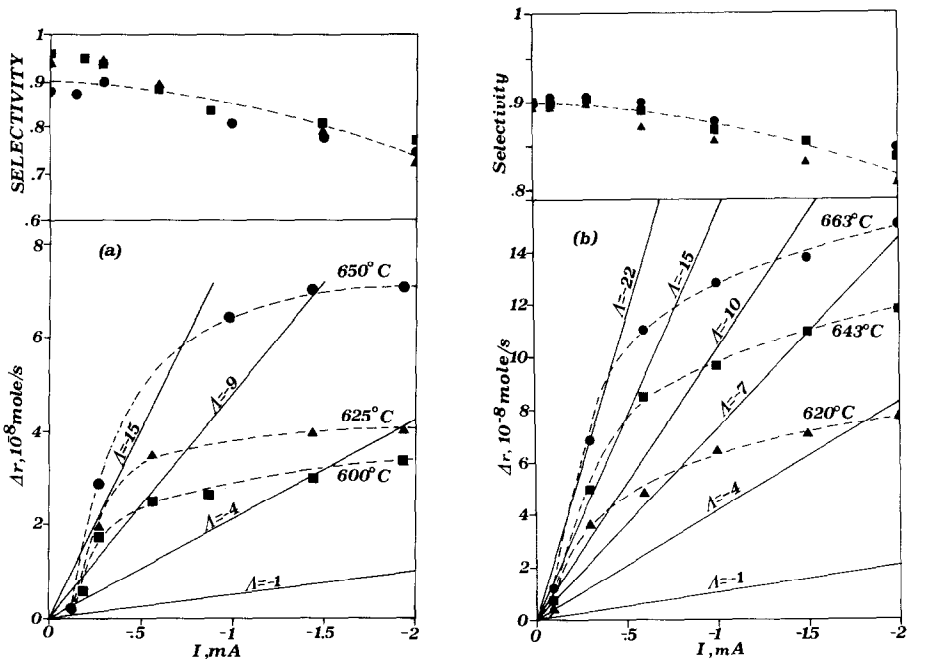

FIG. 7. Steady-state effect of current on the rate of formation of H_2CO and on the selectivity to H_2CO. Solid lines are consant enhancement factor Λ_{H_2CO} lines. (a) Catalyst 1, (b) catalyst 2.

As already mentioned the increase in the rate of CH_4 formation is mostly Faradaic and the exponential dependence of r_{CH_4} on η is a direct consequence of the linear dependence of r_{CH_4} on I (Fig. 5) and of the quasilinear dependence of ln I on η at sufficiently negative η values (Fig. 3).

The parameters A_{H_2CO} and A_{CO} are, like A_{CH_4}, on the order of F/RT, as discussed below. The parameters η^*, which are simply defined as the η values where the rates start to increase exponentially with η, are on the order of -100 to -400 mV for this reaction system. As discussed below the η^* values correspond to specific catalyst potentials V^*_{WR}, which are proportional to T and are characteristic for each reaction.

Effects of Catalyst Potential V_{WR}

The IR-free catalyst potential V_{WR} with respect to the reference Ag electrode, which is in contact with air, is related to the overpotential η through

$$V_{WR} = V^o_{WR} + \eta \qquad (5)$$

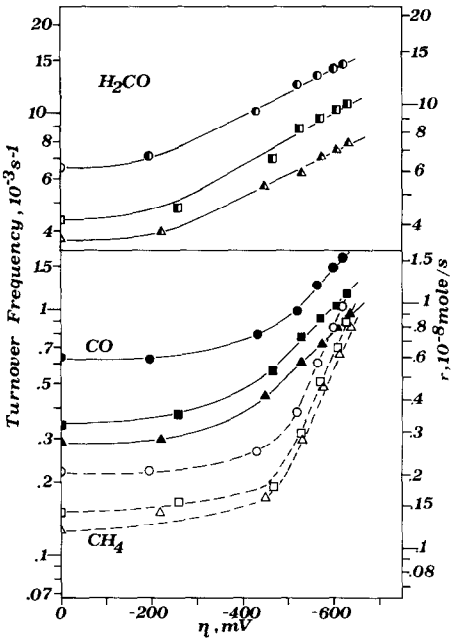

FIG. 8. Effect of catalyst–solid electrolyte activation overpotential η or r_{H_2CO}, r_{CO}, and r_{CH_4}, $P_M = 5 \times 10^{-2}$ bar. ▲ ▲ △, T = 620°C; ◧ ■ □, T = 643°C; ◐ ● ○, T = 663°C. Catalyst 2.

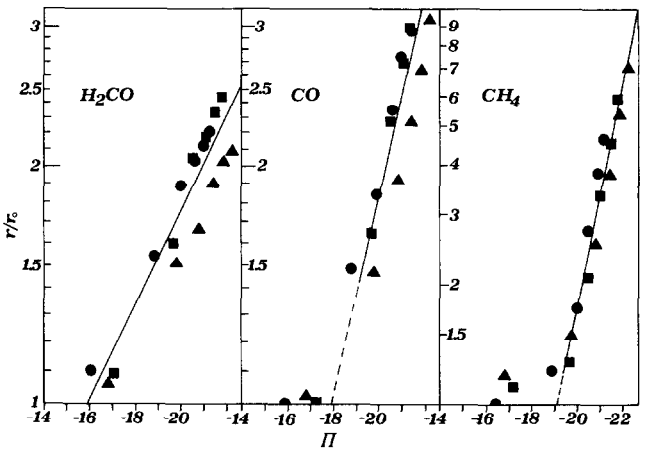

FIG. 9. Effect of the parameter $\Pi = FV_{WR}/RT$ on the rates of formation of H_2CO, CO, and CH_4. Conditions as in Fig. 8. ▲, T = 620°C; ■, T = 643°C; ●, T = 663°C.

where V^0_{WR} is the open-circuit cell emf. The catalyst potential V_{WR} has been recently reported to play a central role in describing the NEMCA effect during C_2H_4 oxidation on Pt (*15, 20*). The same applies here. It was found that the effects of V_{WR} and temperature on the rates can be unified in a single parameter Π defined as

$$\Pi = FV_{WR}/RT \qquad (23)$$

This is shown in Fig. 9, which demonstrates that the logarithms of $r_{H_2CO}/r_{o,H_2CO}$ and $r_{CO}/r_{o,CO}$ depend linearly on Π. As shown in the same figure this also applies for $r_{CH_4}/r_{o,CH_4}$, but it is worth noting that this is simply a consequence of the high-field approximation of the Butler–Volmer equation, since CH_4 is formed mainly by the electrocatalytic reaction (21). The slopes of the plots, i.e., α_{H_2CO}, α_{CO}, and α_{CH_4} are 0.14, 0.30, and 0.65, respectively. The corresponding intersects with the abscissa are $\Pi^*_{H_2CO} = -16$, $\Pi^*_{CO} = -18$, and $\Pi^*_{CH_4} = -19.2$, respectively. Over the temperature range of this study these parameters are essentially independent of temperature as shown in Fig. 9. Consequently, according to Eq. (23) the catalyst potentials V^*_{WR}, below which the rates start increasing exponentially with decreasing catalyst potential, are proportional to T. At T = 916 K the corresponding V^*_{WR} values are −1.26, −1.42, and −1.52 V for H_2CO, CO, and CH_4 formation, respectively. Although, similarly to the case of C_2H_4 oxidation on Pt (*15*), the V^*_{WR} values for H_2CO and CO formation can be considered to be characteristic of the corresponding *catalytic* reactions, i.e., methanol dehydrogenation and decomposition on Ag, no such meaning can be attributed to V^*_{WR,CH_4}, the value of which is expected to also depend on the exchange current density of the catalyst–solid electrolyte interface.

Despite the different origin of the exponential rate dependence on the parameter Π, i.e., NEMCA effect for the formation of H_2CO and CO and simple electrocatalysis for the formation of CH_4, one can summarize the observed kinetic behavior by the following equations:

$$\ln(r_{H_2CO}/r_{o,H_2CO}) = \alpha_{H_2CO}(\Pi^*_{H_2CO} - \Pi),\ \Pi < \Pi^*_{H_2CO} \qquad (24a)$$

$$\ln(r_{CO}/r_{o,CO}) = \alpha_{CO}(\Pi^*_{CO} - \Pi),\ \Pi < \Pi^*_{CO} \qquad (24b)$$

$$\ln(r_{CH_4}/r_{o,CH_4}) = \alpha_{CH_4}(\Pi^*_{CH_4} - \Pi),\ \Pi < \Pi^*_{CH_4} \qquad (24c)$$

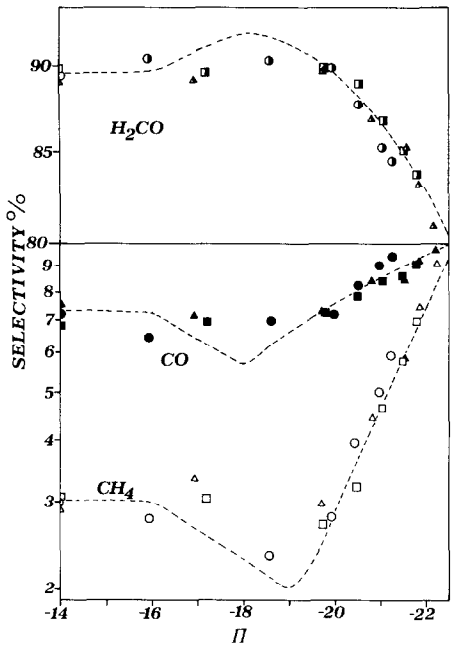

FIG. 10. Effect of the parameter $\Pi = FV_{WR}/RT$ on the selectivity to H_2CO, CO, and CH_4. Conditions and symbols as in Fig. 8; dashed lines from Eq. (24).

It should be noted that from the definition of η and Π, i.e., Eqs. (5) and (23), it is $\Pi_i^* = F(V_{WR}^o + \eta_i^*)/RT$ for all three reactions.

Figure 10 shows the effect of Π on the selectivities S_{H_2CO}, S_{CO}, and S_{CH_4}. The dashed lines result from plots of Eqs. (24). Intermediate Π values lead to a small increase in S_{H_2CO}, but at highly negative Π values S_{H_2CO} decreases exponentially with a concomitant exponential increase in S_{CO} and S_{CH_4}.

NEMCA Effect on Reaction Order and Apparent Activation Energies

As shown in Fig. 11 the NEMCA effect changes not only reaction rate but reaction order as well. Thus, under open-circuit conditions, i.e, $\eta = 0$ (open symbols), the production of H_2CO is zero order in CH_3OH for $P_M > 5 \times 10^{-3}$ bar. However, at $\eta = -650$ mV, the rate becomes between half and first order in methanol for P_M as high as 5×10^{-2} bar, similar to the behavior of r_{CO} and r_{CH_4} as shown in the same figure.

This can be qualitatively understood by noting that the NEMCA effect enhances the rates of surface dehydrogenation and decomposition reactions but probably not the rate of methanol adsorption (*15*). Similarly, increasing negative potentials enhance the electrocatalytic formation of CH_4. Consequently at high negative overpotentials where the surface reactions become very fast, methanol adsorption will tend to become rate limiting. This would then lead to a transition from zeroth order to linear kinetics as is experimentally observed.

By studying the temperature dependence of r_{H_2CO}, r_{CO}, and r_{CH_4} at constant overpotentials η, one can examine the effect of η on the apparent activation energies of the three reactions which are computed from standard Arrhenius ln r versus $1/T$ plots. Figure 12 shows the effect of overpotential on the apparent activation energies of r_{H_2CO},

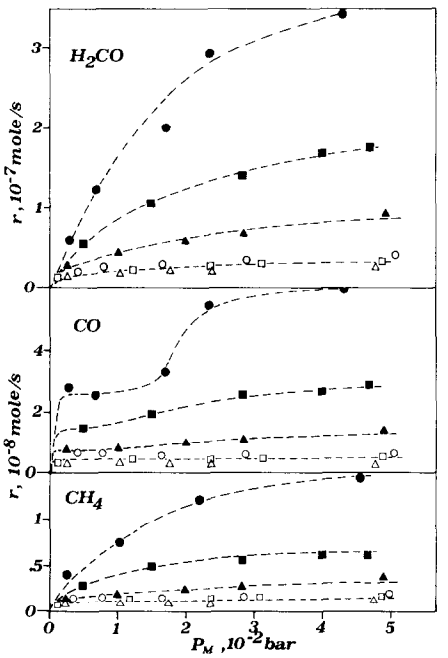

FIG. 11. Effect of CH_3OH partial pressure P_M, on the regular (open symbols) and NEMCA-induced ($\eta = -0.65$ V, filled symbols) catalytic activity for the formation of H_2CO, CO, and CH_4. Triangles, $T = 645$°C; squares, $T = 665$°C; circles, $T = 683$°C.

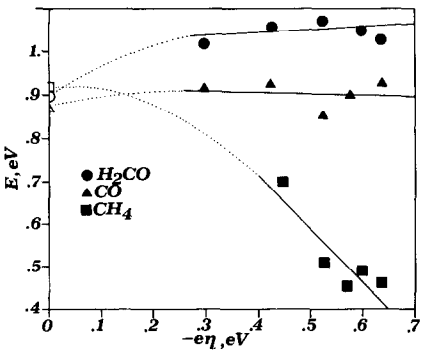

FIG. 12. Effect of overpotential on the apparent activation energies of formation of H_2CO, CO, and CH_4.

r_{CO}, and r_{CH_4}. Increasing $|\eta|$ causes a small increase in E_{H_2CO} and a substantial decrease in E_{CH_4}, while E_{CO} remains practically unaffected. However, it should be noted that, because of the NEMCA-induced change in reaction order discussed above, the E values extracted from ln r versus $1/T$ plots are only apparent overall activation energies and cannot be attributed specifically to any single reaction step. The observed decrease in E_{CH_4} with increasing $|\eta|$ is in good qualitative agreement with the classical theory of electrocatalytic reactions (*30*). Significant changes in the activation energy of catalytic reactions with changing catalyst work function have been found for both metallic (*15*) and nonmetallic (*31*) catalysts.

DISCUSSION

Main Results

1. The catalytic rates of CH_3OH dehydrogenation and decomposition on Ag can be reversibly enhanced by a factor of 5 to 10 by removing oxygen anions from the Ag catalyst surface. The observed increase in the rate of dehydrogenation is typically 15 times higher than the rate of O^{2-} removal from the catalyst. The effect is non-Faradaic and induces significant changes in product selectivity. At more negative potentials the electrocatalytic rate of CH_4 formation from CH_3OH is also enhanced.

2. The rates of H_2CO, CO, and CH_4 formation increase exponentially with decreasing catalyst potential V_{WR} below three threshold potential values V^*_{WR}. As catalyst potential decreases, the threshold value for dehydrogenation to H_2CO is reached first ($\Pi^* = -16$), followed by those for decomposition to CO ($\Pi^* = -18$) and for CH_4 formation ($\Pi^* = -19.2$). The Π^* value for CH_4 formation depends on the polarizability of the catalyst–solid electrolyte interface and therefore should not be considered as characteristic of the methane formation reaction, contrary to the Π^* values corresponding to the catalytic reactions of dehydrogenation and decomposition on the Ag surface. The exponential rate increase for dehydrogenation is the least steep ($\alpha_{H_2CO} = 0.14$), while those for decomposition to CO and CH_4 formation are much steeper ($\alpha_{CO} = 0.30$ and $\alpha_{CH_4} = 0.65$). Consequently, at more negative catalyst potentials the selectivity to CH_4 increases exponentially with a concomitant decrease in the selectivity to H_2CO.

3. The rate relaxation time constants τ during galvanostatic transients are on the order of $2FN_o/I$, where N_o is the catalyst reactive oxygen uptake measured by reactive oxygen titration with CO (Fig. 6). This shows conclusively that O^{2-} pumping from the catalyst removes negatively charged adsorbed oxygen species from the entire catalyst surface and not only from the vicinity of the catalyst–solid electrolyte–gas phase three-phase boundaries. This behavior has been also observed in all previous studies of the NEMCA effect (*15–20*).

Estimation of Enhancement Factors

The magnitude of the enhancement factors Λ_j, where the index $j = 1, 2$ stands for the catalytic reactions of H_2CO and CO formation, respectively, is determined mainly by the magnitude of the open-circuit rates $r_{o,j}$ and of the exchange current. Since different reactions have been found to exhibit dramatically different Λ values (Table 3) it becomes important to understand the origin of these differences and also to describe how Λ is influenced by the catalyst surface

TABLE 3

Catalytic Reactions Found to Exhibit the NEMCA Effect

Reactant	Product	Catalyst	T (°C)	Λ range	Reference
1. CH_2CH_2, O_2	Ethylene oxide, CO_2	Ag	320–420	[0, +300]	(*16, 17*)[a]
2. Propylene, O_2	Propylene oxide, CO_2	Ag	320–420	[0, +300]	(*18*)[a]
3. $CH_2{=}CH_2$, O_2	CO_2	Pt	260–420	[0, $+3 \times 10^5$]	(*15, 20*)
4. CO, O_2	CO_2	Pt	300–550	[−500, +500]	(*19*)
5. CH_3OH, O_2	CO_2, H_2CO	Pt	400–500	[-3×10^4, $+10^4$]	(*29*)[a]
6. CH_3OH	H_2CO, CO, CH_4	Pt	400–500	[−10, 0]	(*29*)[a]
7. CH_3OH	H_2CO, CO, CH_4	Ag	550–700	[−25, 0]	This work[a]

[a] Change in product selectivity observed.

area and by the catalyst–solid electrolyte exchange current.

In a recent paper (*15*) it has been shown that for anodic operation, i.e., O^{2-} pumping to the catalyst, the enhancement factor Λ is on the order of $2Fr_o/I^o$, where I^o is defined as the current at an overpotential equal to η^*. This was derived by using the high-field approximation of the Butler–Volmer equation and by assuming that the anodic transfer coefficient α_a equals the slope α of the $\ln(r/r_o)$ versus Π plots. By making the same assumption in the present case of cathodic operation one can show that Λ_j must be on the order of $-2Fr_{o,j}/I_j^o$. The parameters I_j^o can be directly obtained from Fig. 3 for $\eta^*_{H_2CO} = -0.2$ V and $\eta^*_{CO} = -0.4$ V. Thus, one computes that at 665°C it should be $\Lambda_{H_2CO} \approx -120$ and $\Lambda_{CO} \approx -5$. The latter value is in good agreement with experiment but $|\Lambda_{H_2CO}|$ is significantly overestimated because the assumption $\alpha_{H_2CO} = \alpha_c$ is rather inaccurate in this case where α_{H_2CO} is very small (= 0.14).

Although the parameters $-2Fr_{o,j}/I_j^o$ can provide only an estimate of the order of magnitude of Λ_j they are useful in assessing the effect of intrinsic turnover rate, catalyst surface area, and catalyst–solid electrolyte exchange current density on Λ. By noting that r_o is proportional to the catalyst surface area and also that the parameter I^o is proportional to the catalyst–solid electrolyte exchange current I_o (*15*), one can conclude that for a given reaction, temperature, and gaseous composition the enhancement Λ is proportional to the intrinsic catalytic turnover rate and to the catalyst surface area and inversely proportional to the exchange current density of the catalyst–solid electrolyte interface. Consequently, to observe the NEMCA effect and obtain high $|\Lambda|$ values one must have a relatively fast catalytic reaction and a polarizable catalyst–solid electrolyte interface.

Origin of NEMCA Effect and of Exponential Dependence of Catalytic Rates on V_{WR}

To explain the experimental observation

$$\ln(r_j/r_{j,o}) = \alpha_j F(V^*_{WR,j} - V_{WR})/RT \quad (25)$$

which has been found to describe the NEMCA effect for the present work and for all other systems where the effect of O^{2-} pumping on catalysts has been studied with simultaneous accurate measurement of the overpotential η and of the catalyst potential V_{WR} (*15, 20*), one must first examine what is the effect of O^{2-} pumping and of the appearance of activation overpotential η on the electronic properties of the metal catalyst. This question has been addressed in detail in a recent communication which described the NEMCA effect during C_2H_4 oxidation on Pt (*15*). It was shown that the

catalyst potential with respect to the reference electrode, i.e., V_{WR}, is given from

$$V_{WR} = (\bar{\mu}_{e,R} - \bar{\mu}_{e,W})/e = (\Phi_W - \Phi_R) + (\Psi_W - \Psi_R) \quad (26)$$

where $\bar{\mu}_{e,W}$, $\bar{\mu}_{e,R}$, $e\Phi_W$, $e\Phi_R$, and Ψ_W, Ψ_R are the electrochemical potentials of electrons (or Fermi levels), work functions, and outer (Volta) potentials, respectively, of the catalyst (W) and reference (R) electrodes. The Ψ, or Volta, potentials are nonzero only when there is a net charge on the metal catalyst plus adsorbed layer. Consequently the Ψ terms are frequently neglected in the catalytic literature. Equation (26) is valid under both open-circuit and close-circuit conditions. For open-circuit (i.e., SEP) measurements it implies that the open-circuit emf V^{o}_{WR} provides a measure of the catalyst work function in relation to the reference electrode work function, provided that no net charge develops on the two electrodes, i.e., $\Psi_W = \Psi_R = 0$.

Under closed-circuit conditions, i.e., during O^{2-} pumping, the reference electrode remains unaffected, i.e., $\bar{\mu}_{e,R}$, Φ_R, and Ψ_R remain constant. One can therefore rewrite Eq. (26) as

$$\eta = V_{WR} - V^{o}_{WR} = (\bar{\mu}_{e,W(I=0)} - \bar{\mu}_{e,W(I)})/e = (\Phi_{W(I)} - \Phi_{W(I=0)}) + (\Psi_{W(I)} - \Psi_{W(I=0)}). \quad (27)$$

The preceding equation has been derived rigorously (*15*) and without making any assumptions. To further exploit Eq. (27) it is necessary to make some assumption regarding the magnitude of the last term $\Psi_{W(I)} - \Psi_{W(I=0)}$ on the catalyst surface exposed to the gas phase. First it is worth noting that $\bar{\mu}_{e,W}$ is the same throughout the bulk of the metal catalyst. However, Φ_W and Ψ_W, the sum of which equals $-\bar{\mu}_{e,W}/e$, need not be the same over the entire catalyst surface if the catalyst electrode carries a net charge which is not uniformly distributed on the catalyst surface. Such a net charge may exist but will be localized at the metal–solid electrolyte interface, which is usually modeled as a resistor and a capacitor connected in parallel. However, what is of interest here are changes in Φ_W and Ψ_W on the metal–electrode surface which is catalytically active, i.e., which is exposed to the gas phase. Any ions or molecules directly adsorbing on the catalytically active surface will be paired with a compensating charge in the metal. The effect of such ion–electron pairs produced by adsorption from the gas phase would be included in a work function measurement and therefore must be included within Φ_W and not Ψ_W. Consequently when the Φ_W and Ψ_W terms in Eqs. (26) and (27) refer to the catalytically active surface of the catalyst electrode, then the Ψ_W terms vanish and one can rewrite these equations as

$$V_{WR} = \Phi_W - \Phi_R \quad (28)$$

$$\eta = V_{WR(I)} - V_{WR(I=0)} = \Phi_{W(I)} - \Phi_{W(I=0)}. \quad (29)$$

Equation (29) implies that when $\eta > 0$, i.e., $V_{WR(I)} > V_{WR(I=0)}$, or equivalently when O^{2-} is pumped *to* the catalyst surface, then there is an increase in catalyst work function. This has been found to cause dramatic non-Faradaic increases in the rates of C_2H_4 and C_3H_6 epoxidation and complete oxidation (*16–18*), CO oxidation on Pt (*19*), and C_2H_4 complete oxidation on Pt (*15, 20*) (Table 3). This dramatic rate enhancement has been explained semiquantitatively by considering the decrease in bonding strength of chemisorbed species resulting from the increase in catalyst work function (*15*).

In the present investigation exactly the opposite behavior is observed, i.e., significant non-Faradaic rate enhancements are obtained when O^{2-} is pumped *from* the catalyst surface, which corresponds to $\eta < 0$, i.e., $V_{WR(I)} < V_{WR(I=0)}$. According to Eq. (29) this implies a *decrease* in catalyst work function.

At the molecular level the induced decrease in catalyst work function is due to the depletion of O^{2-} from the catalyst–solid electrolyte interface and from the concomi-

tant removal of partially or completely ionized oxygen initially bonded all over the entire catalyst surface. Oxygen chemisorption on polycrystalline Ag is known to produce at least three distinct oxygen species (*23–25*), which have been attributed to molecularly adsorbed, atomically adsorbed, and subsurface oxygen (*23*). The exact role of each of these types of oxygen on the mechanism of Ag-catalyzed oxidation reactions has been the subject of intensive study and controversy, but it is almost universally accepted that atomically bonded and subsurface oxygen carry negative charges between 0 and −2 (*23–25*). Depletion of completely or partially ionized species with negative charges from a catalyst surface is well known to produce a positive surface potential change, i.e., a decrease in catalyst work function (*26*). The situation is depicted schematically in Fig. 13, where no attempt was made to show the compensating charges in the metal.

The decrease in catalyst work function increases the Fermi level and electrochemical potential of electrons in the catalyst (*26*) and therefore increases the availability of electrons for chemisorptive bond formation. This leads to stronger bonding between the catalyst and chemisorbed species with a concomitant increase in the heats of chemisorption. According to early theoretical considerations of Boudart (*27*) it should be

$$\Delta(-\Delta H_{ad}) = -(n/2)e\Delta\Phi \qquad (30)$$

where n is the number of valence electrons of the adatom taking part in the bonding. Despite its simplicity, Eq. (30) has been found in several occasions to be in good agreement with experiment (*27*). For the case of CH_3OH chemisorption on Ag it is fairly well established that adsorption proceeds via formation of a methoxy group (*24, 28*); therefore, a reasonable approximation would be $n = 1$. Equation (30) pre-

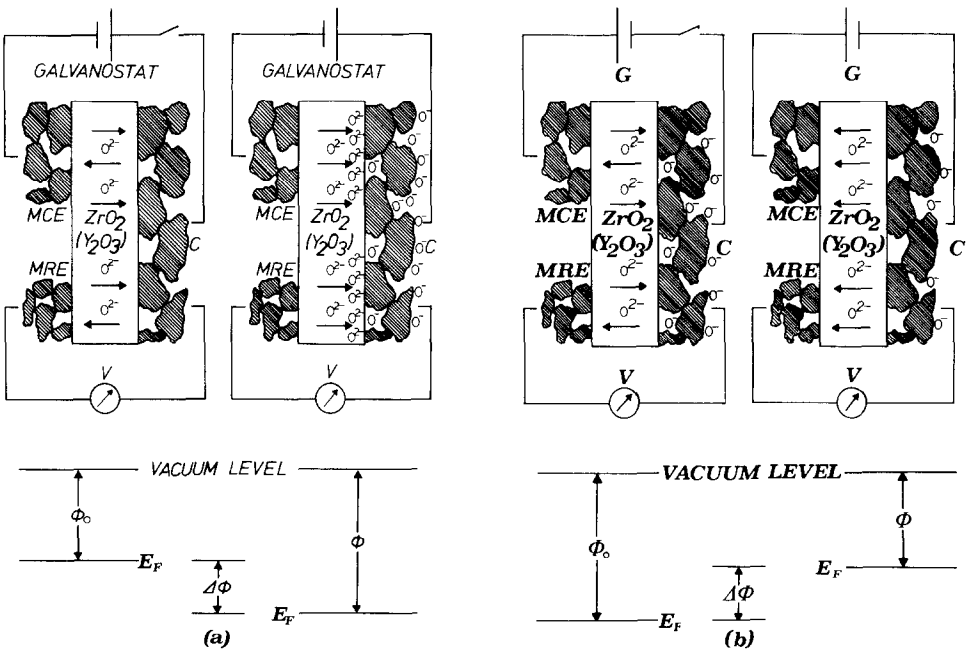

FIG. 13. Schematic representation of the effect of positive (a) and negative (b) currents on the relative concentration of oxygen anions on the catalyst surface and on the corresponding changes in Fermi level E_F and in work function Φ when $\Psi = 0$. C, catalyst; MCE, metal counter electrode; MRE, metal reference electrode.

dicts a substantial increase in the heat of chemisorption of CH_3OH with decreasing catalyst work function, i.e., when O^{2-} is pumped *from* the catalyst. It is not surprising then that O^{2-} pumping *from* the catalyst is found experimentally to cause a dramatic increase in the rates of CH_3OH dehydrogenation and decomposition. This is exactly what one would expect for decomposition reactions if the nature of the activated complexes leading to product formation is not changing substantially. Furthermore, one can explain the exponential dependence of the rates on η and V_{WR} by noting that η and V_{WR} are linearly related to the changes in catalyst work function $e\Delta\Phi$ [Eq. (29)] and, therefore, to the induced changes in the heats of adsorption [Eq. (30)] which are expected from classical activated complex kinetic considerations to induce exponential changes in the catalytic rates (*15*).

The order in which r_{H_2CO} and r_{CO} start increasing with decreasing V_{WR} (Fig. 9), thus decreasing work function $e\Phi$, is also reasonable in view of the above discussion. Thus it is the dehydrogenation reaction that takes off first, followed by the decomposition to CO, which involves abstraction of two more H atoms and requires even more negative catalyst potentials.

Table 3 summarizes the reactions where the NEMCA effect has been studied so far. One can distinguish two groups of reactions. The first group consists of reactions exhibiting a positive NEMCA effect, i.e., rate acceleration by O^{2-} pumping *to* the catalyst ($I > 0$, $\eta > 0$, $\Lambda > 0$) which, as discussed above, corresponds to an *increase* in catalyst work function. In some of these reactions (*16–18*) negative currents cause a decrease in the rate.

The second group contains reactions exhibiting a negative NEMCA effect, i.e., rate enhancement upon O^{2-} removal *from* the catalyst ($I < 0$, $\eta < 0$, $\Lambda < 0$), which corresponds to a decrease in catalyst work function.

It is interesting to note that the first class contains mostly oxidation reactions, while the second class contains mostly decomposition reactions. The oxidation of CO on Pt, which belongs to both groups, depending on catalyst potential, is no exception to this rule, since it exhibits a negative NEMCA effect at very negative catalyst potentials where the reaction proceeds via CO disproportionation on the catalyst surface followed by carbon combustion (*19*). The oxidation of CH_3OH on Pt exhibits similar behavior, but little is known about its mechanism yet (*29*).

It is tempting to propose the terms electrophobic and electrophilic respectively for these two groups of reactions, since they are accelerated by a decrease or increase respectively in the electrochemical potential of metal electrons and by a concomitant decrease or increase in catalyst electron availability for chemisorptive bond formation.

CONCLUSIONS

The catalytic activity of Ag for the conversion of CH_3OH to H_2CO and CO can be markedly enhanced by electrochemically removing oxygen anions from the catalyst surface. The induced non-Faradaic electrochemical modification of catalytic activity (NEMCA) leads to rate enhancements up to 600% which are accompanied by significant changes in product selectivity. The increase is 10–15 times higher than the rate of O^{2-} removal from the catalyst. As in previous studies (*15–20*) the observed enhancement factors Λ are of order $2Fr_o/I^o$ where r_o is the regular catalytic rate and I^o is proportional to the exchange current of the catalyst–solid electrolyte interface. Over certain ranges of catalyst potential, the catalytic reaction rates increase exponentially with decreasing catalyst potential.

The above observations can be accounted for by considering the decrease in catalyst work function resulting from the depletion of oxygen anions from the catalyst–solid electrolyte interface and from the catalyst surface. This is a generalization of

the first proposed explanation of the NEMCA effect observed during ethylene and propylene epoxidation on Ag (*16–18*). In these early studies it was proposed that O^{2-} pumping to or from Ag surfaces leads to formation and depletion, respectively, of some surface species AgO*. More recent studies of the NEMCA effect (*15, 19, 20*), including the present work, strongly support the idea that O* is simply O^-.

This reaction system provides an example of a negative NEMCA effect, i.e., catalytic rate enhancement due to oxygen anion removal from the catalyst and, consequently, due to a decrease in catalyst work function.

The observed phenomena show the usefulness of solid electrolyte cells in influencing and controlling the electronic and catalytic properties of metal catalysts. The use of surface spectroscopic techniques to examine *in situ* catalytic surfaces subject to O^{2-} pumping could lead to complete elucidation of the NEMCA effect, which is of considerable theoretical and practical importance.

ACKNOWLEDGMENTS

Financial support from the VW Stiftung of the Federal Republic of Germany and from the European Economic Community Nonnuclear Energy Program is gratefully acknowledged. We also thank Professor L. Riekert of the University of Karlsruhe for helpful discussions and our reviewer No. 1 for some very thoughtful suggestions.

REFERENCES

1. Vayenas, C. G., "Proceedings, 6th International Conference on Solid State Ionics, Garmish-Partenkirchen, September 1987," *Solid State Ionics* **28–30,** 1521 (1988).
2. Stoukides, M., *Ind. Eng. Chem. Res.* **27,** 1745 (1988).
3. Stoukides, M., and Vayenas, C. G., *J. Catal.* **64,** 18 (1980).
4. Stoukides, M., and Vayenas, C. G., *J. Catal.* **74,** 266 (1982).
5. Stoukides, M., and Vayenas, C. G., *J. Catal.* **82,** 45 (1983).
6. Häfele, E., and Lintz, H.-G., *Ber. Bunsenges. Phys. Chem.* **90,** 288 (1986).
7. Vayenas, C. G., Lee, B., and Michaels, J. N. *J. Catal.* **66,** 36 (1980).
8. Vayenas, C. G., Georgakis, C., Michaels, J. N., and Tormo, J., *J. Catal.* **67,** 348 (1981).
9. Yentekakis, I. V., Neophytides, S., and Vayenas, C. G., *J. Catal.* **111,** 152 (1988).
10. Stoukides, M., Seimanides, S., and Vayenas, C. G., *ACS Symp. Ser.* **196,** 165 (1982).
11. Pancharatnam, S., Huggins, R. A., and Mason, D. M., *J. Electrochem. Soc.* **122,** 869 (1975).
12. Gür, T. M., and Huggins, R. A., *J. Electrochem. Soc.* **126,** 1067 (1979).
13. Gür, T. M., and Huggins, R. A., *Science* **219,** 967 (1983).
14. Gür, T. M., and Huggins, R. A., *J. Catal.* **102,** 443 (1986).
15. Bebelis, S., and Vayenas, C. G., *J. Catal.* (1989).
16. Stoukides, M., and Vayenas, C. G., *J. Catal.* **70,** 137 (1981).
17. Stoukides, M., and Vayenas, C. G., *ACS Symp. Ser.* **178,** 181 (1982).
18. Stoukides, M., and Vayenas, C. G., *J. Electrochem. Soc.* **131,** 839 (1984).
19. Yentekakis, I. V., and Vayenas, C. G., *J. Catal.* **111,** 170 (1988).
20. Vayenas, C. G., Bebelis, S., and Neophytides, S., *J. Phys. Chem.* **92,** 5083 (1988).
21. Manton, M., Ph.D. thesis, MIT, 1986.
22. Wang, D. Y., and Nowick, A. S., *J. Electrochem. Soc.* **126,** 1155 (1979).
23. Bao, X., Deng, J., and Dong, S., *Surf. Sci.* **163,** 444 (1985).
24. Wachs, I. E., and Madix, R. J., *Surf. Sci.* **76,** 531 (1978).
25. Kilty, P. A., Rol, N. C., and Sachtler, W. M. H., *in* "Proceedings, 5th International Congress on Catalysis, Palm Beach, 1972" (J. Hightower, Ed.). North-Holland, Amsterdam, 1972.
26. Gundry, P. M., and Tompkins, F. C., *in* "Experimental Methods in Catalytic Research" (R. B. Anderson, Ed.). Academic Press, New York, 1968.
27. Boudart, M., *J. Amer. Chem. Soc.* **74,** 3556 (1952).
28. Bao, X., and Deng, J., *J. Catal.* **99,** 391 (1986).
29. Neophytides, S., and Vayenas, C. G , in preparation.
30. Bockris, J. O'M., and Reddy, A. K. N., *in* "Modern Electrochemistry," Plenum/Rosetta, New York, 1973.
31. Krylov, O. V., "Catalysis by Nonmetals." Academic Press, New York, 1971.